PCCP

Accepted Manuscript

ROYAL SOCIETY OF CHEMISTRY

www.rsc.org/pccp

ARTICLE TYPE www. rsc.org/xxxxxx | XXXXXXXX

Quantum dynamics of the photostability of pyrazine†

Matthieu Sala,*[a] Stéphane Guérin[a] and Fabien Gatti[b]

Received Xth XXXXXXXXXX 20XX, Accepted Xth XXXXXXXXX 20XX
First published on the web Xth XXXXXXXXXX 200X
DOI: 10.1039/b000000x

We investigate the radiationless decay of photoexcited pyrazine to its ground electronic state using multireference electronic structure and quantum dynamics calculations. We construct a quadratic vibronic coupling Hamiltonian, including the four lowest electronic states and ten vibrational modes, by fitting against more than 5000 *ab-initio* points. We then use this model to simulate the non-adiabatic excited state dynamics of the molecule using the multi-configuration time-dependent Hartree method. On the basis of these calculations, we propose a new mechanism for this decay process involving a conical intersection between the $A_u(n\pi^*)$ state and the ground state. After excitation to the $B_{2u}(\pi\pi^*)$ state, the molecule decays to both the $B_{3u}(n\pi^*)$ and $A_u(n\pi^*)$ states on an ultrashort time scale of approximately 20 fs. The radiationless decay to the ground state then occurs from the $A_u(n\pi^*)$ state on a much longer time scale.

1 Introduction

The dynamics of molecular systems in excited electronic states is an important topic in modern physical chemistry. After electronic excitation, many molecules undergo ultrafast radiationless decay processes, resulting from the existence of regions of the nuclear configuration space where two or more potential energy surfaces are degenerate. These features, known as conical intersections,[1,2] are associated with a strong coupling between the electronic and nuclear motions, and hence, with a breakdown of the Born-Oppenheimer approximation.

Our understanding of these ultrafast non-adiabatic processes, often occurring on a sub-picosecond time scale, has greatly benefited from the development of time-resolved spectroscopic techniques,[3–5] and efficient computational methods.[6–9]

Pyrazine is a benchmark system for the study of non-adiabatic effects occurring at conical intersections. Its UV spectrum[10–16] exhibits a broad band dominated by a transition to the $B_{2u}(\pi\pi^*)$ state, indicating a large density of states characteristic of the existence of strong vibronic couplings with lower electronic states. Time-resolved photoelectron spectroscopy studies[17–19] revealed the existence of two time constants. The first one, of approximately 20 fs, is associated with an ultrafast internal conversion process occurring from the $B_{2u}(\pi\pi^*)$ state. The second one, of approximately 20 ps, has been ascribed to a subsequent internal conversion process leading the molecule back to its ground electronic state.

From the theoretical point of view, numerous studies of the excited electronic state energies and properties based on high-level electronic structure calculations have been reported.[20–27] The UV spectrum and the excited state nuclear dynamics of the molecule have been studied using reduced[28–36] and full dimensional[37–42] quantum dynamics, as well as various semi-classical dynamics methods.[43–54] Pyrazine has also been used as a convenient model system for the study of the laser control of non-radiative transitions at conical intersections.[55–63]

In most previous theoretical studies of the photophysics of pyrazine, only the bright $B_{3u}(\pi\pi^*)$ and $B_{2u}(\pi\pi^*)$ electronic states were considered. In 2008, trajectory surface hopping (TSH) simulations based on time-dependent density functional theory (TDDFT) electronic structure calculations performed by Bonačić-Koutecký *et al.*[52] suggested that the low-lying dark $A_u(n\pi^*)$ and $B_{2g}(n\pi^*)$ states were significantly populated through internal conversion from the bright $B_{2u}(\pi\pi^*)$ state in a time scale of a few tens of femtoseconds. Further works based on TSH[54] and wavepacket propagation simulations[35] reported a significant internal conversion to the $A_u(n\pi^*)$ state, but not to the $B_{2g}(n\pi^*)$ state. However, very recently, Fujimura *et al.*[36] questioned these results based on multi-reference configuration interaction (MRCI) calculations and wavepacket propagation simulations. They claimed that the internal conversion process to the $A_u(n\pi^*)$ state previously reported was a consequence of the "poor accuracy" of the

† Electronic Supplementary Information (ESI) available containing the numerical values of all the parameters of the vibronic coupling model Hamiltonian used in this paper, and quantum dynamics simulations illustrating the influence of the position of the $A_u(n\pi^*)$ state on the efficiency of the internal conversion process occuring to this state in the first tens of femtosecond after excitation.

[a] *Laboratoire Interdisciplinaire Carnot de Bourgogne UMR 6303 CNRS, Université de Bourgogne Franche-Comté, BP 47870, F-21078 Dijon, France. E-mail: matthieu.sala@u-bourgogne.fr.*
[b] *CTMM, Institut Charles Gerhardt UMR 5253 CNRS, CC 15001, Université Montpellier 2, F-34095 Montpellier, France*

TDDFT and extended multi-configuration quasi-degenerate second order perturbation theory (XMCQDPT2) electronic structure calculation methods used in refs.[52] and[35] respectively. This disagreement is discussed in the present paper (see Section 2 below).

The decay of the molecule to its ground electronic state observed experimentally after excitation to the $B_{2u}(\pi\pi^*)$ state, has been less intensively investigated. Yamazaki *et al.* measured a lifetime of 25 ps for the high-lying vibronic levels of the first singlet excited state.[10] Wang *et al.* used femtosecond time-resolved photoelectron imaging to follow the decay of the molecule after electronic excitation.[17] At a pump wavelength of 264 nm ($\sim$ 4.70 eV), they measured a decay time constant of 22 ps and ascribed it to an internal conversion process from the first singlet excited state to the ground state. Stert *et al.*, using similar techniques, measured a decay time constant of 22 ps at a pump wavelength of 266.7 nm ($\sim$ 4.65 eV) and a decay time constant of 17.5 ps at a slightly lower excitation wavelength of 261.3 nm ($\sim$ 4.75 eV).[18] Again, this decay process was interpreted as an internal conversion process to the ground state. The authors analyzed these results in light of the theoretical work of Domcke *et al.*,[64] who demonstrated the existence of a conical intersection between the first excited singlet state and the ground state at a geometry similar to the so-called prefulvene conical intersection responsible for the "channel 3" phenomenon in benzene (see Section 3).[65–73] In their recent TSH study,[54] Mitrić *et al.* found a minor radiationless decay of the molecule to the ground state during the first 200 fs after excitation to the bright $B_{2u}(\pi\pi^*)$ state, occuring through a ring-puckering coordinate leading to a low-lying S_1/S_0 conical intersection, in agreement with the work of Domcke *et al.*.[64]

In this paper, we propose an alternative mechanism for this decay process to the ground electronic state, involving a conical intersection between the $A_u(n\pi^*)$ state and the ground state. To support this hypothesis, we present quantum dynamics simulations, performed using the multi-configuration time-dependent Hartree (MCTDH) method,[74–77] based on a quadratic vibronic coupling model Hamiltonian[78] including the four lowest electronic states and ten vibrational modes. The model is constructed via fitting to the results of extensive *ab-initio* electronic structure calculations performed with the complete active space self-consistent field (CASSCF) and XMCQDPT2 methods.[79]

The rest of this paper is organized as follows: the vibronic coupling model Hamiltonian used in this work is presented in Section 2, the decay pathways to the ground state are analyzed using electronic structure calculations in Section 3, the multi-configuration time-dependent Hartree method, used for the quantum dynamics calculations is briefly presented in Section 4, simulations of the UV absorption spectrum and the excited state dynamics of the molecule are presented and discussed in Section 5 and Section 6 concludes the paper.

2 The model Hamiltonian

The usual adiabatic representation for the electronic states is not adapted for the study of the excited state non-adiabatic dynamics of molecular systems because, in this representation, the derivative coupling terms have a singular behavior at conical intersections, and the corresponding regions of the potential energy surfaces have a complicated topography.[78,80,81] In this case, it is more convenient to work in a so-called quasidiabatic representation, which is obtained from the adiabatic representation through a unitary transformation designed to minimize the derivative coupling terms, such that they can be neglected. In this representation, the electronic couplings appear as scalar, potential-like operators, and the potential matrix elements have a simple and smooth topography. As usual, the quasidiabatic representation will be simply termed diabatic representation in the rest of this paper.

We used the quadratic vibronic coupling model of Köppel *et al.*.[78] In this model, the diabatic Hamiltonian $\boldsymbol{H_0}(\boldsymbol{Q})$, written as a function of dimensionless normal coordinates[32,78] which are gathered in the vector $\boldsymbol{Q}$, reads

$$\boldsymbol{H_0}(\boldsymbol{Q}) = \sum_i \frac{\omega_i}{2}\left(-\frac{\partial^2}{\partial Q_i^2} + Q_i^2\right)\boldsymbol{I} + \boldsymbol{W}(\boldsymbol{Q}). \tag{1}$$

The first term of this equation is the ground state Hamiltonian in the harmonic approximation multiplied by the identity matrix $\boldsymbol{I}$. The second term is the non-diagonal potential energy matrix, whose elements are expressed as Taylor expansions around a reference geometry $\boldsymbol{Q_0}$, chosen as the ground state equilibrium geometry in this work

$$\begin{aligned} W_{\alpha\alpha}(\boldsymbol{Q}) &= E_\alpha + \sum_i \kappa_i^{(\alpha)} Q_i + \sum_{i,j} \gamma_{ij}^{(\alpha)} Q_i Q_j + \cdots \\ W_{\alpha\alpha'}(\boldsymbol{Q}) &= \sum_i \lambda_i^{(\alpha\alpha')} Q_i + \sum_{i,j} \mu_{ij}^{(\alpha\alpha')} Q_i Q_j + \cdots . \end{aligned} \tag{2}$$

Here, $\alpha \neq \alpha'$, the E_α are the vertical excitation energies, $\kappa_i^{(\alpha)}$ and $\gamma_{ij}^{(\alpha)}$ are respectively the linear and quadratic intrastate coupling constants for the α^{th} electronic state and $\lambda_i^{(\alpha\alpha')}$ and $\mu_{ij}^{(\alpha\alpha')}$ are respectively the linear and quadratic interstate coupling constants between the α^{th} and α'^{th} electronic states. For highly symmetric molecules, such as pyrazine, many of the terms appearing in eq. (2) vanish by symmetry. The non-vanishing linear terms fulfill

$$\Gamma_\alpha \otimes \Gamma_{Q_i} \otimes \Gamma_{\alpha'} \supset A_g, \tag{3}$$

where Γ_α and Γ_{Q_i} denote the irreducible representations of the α^{th} electronic state and of the i^{th} vibrational mode. Similarly,

the non-vanishing quadratic terms fulfill

$$\Gamma_\alpha \otimes \Gamma_{Q_i} \otimes \Gamma_{Q_j} \otimes \Gamma_{\alpha'} \supset A_g. \quad (4)$$

Similar expressions hold for higher-order terms.

The four lowest electronic states, which are the ground, $B_{3u}(n\pi^*)$, $A_u(n\pi^*)$ and $B_{2u}(\pi\pi^*)$ states, and ten out of the twenty-four vibrational modes of the molecule were included in our model. The modes included are those with large first-order coupling constants. Specifically, our model includes the four A_g modes ν_{6a}, ν_1, ν_{9a} and ν_{8a}, the only B_{1g} mode ν_{10a} which couples the $B_{3u}(n\pi^*)$ and $B_{2u}(\pi\pi^*)$ states at first order, the B_{3g} mode ν_{8b} which couples the $B_{3u}(n\pi^*)$ and $A_u(n\pi^*)$ states at first order, the B_{2g} modes ν_4 and ν_5 which couple the $A_u(n\pi^*)$ and $B_{2u}(\pi\pi^*)$ states at first order, and the A_u modes ν_{16a} and ν_{17a} which couple the ground and $A_u(n\pi^*)$ states at first order. The B_{2u} and B_{3u} modes, mediating the coupling between the ground state and the $B_{2u}(\pi\pi^*)$ and $B_{3u}(n\pi^*)$ states, respectively, were not included in our model because the energy separation between them is large enough.

All the first and second order terms were included in the expansion of the potential matrix elements of eq. (2). In addition, some selected third and fourth order terms were included in our model. Specifically, third order terms of the form

$$\begin{aligned} W^{(3)}_{\alpha\alpha}(\boldsymbol{Q}) &= \sum_{i,j} \sigma^{(\alpha)}_{ij} Q_i^2 Q_j \\ W^{(3)}_{\alpha\alpha'}(\boldsymbol{Q}) &= \sum_{i,j} \theta^{(\alpha\alpha')}_{ij} Q_i^2 Q_j, \end{aligned} \quad (5)$$

and diagonal fourth order terms of the form

$$W^{(4)}_{\alpha\alpha}(\boldsymbol{Q}) = \sum_i \eta^{(\alpha)}_i Q_i^4, \quad (6)$$

were included. The linear intrastate coupling constants $\kappa^{(\alpha)}_i$ are reported in Table 1 and the linear interstate coupling constants $\lambda^{(\alpha\alpha')}_i$ and quadratic intrastate coupling constants $\gamma^{(\alpha)}_{ii}$ for the non-totally symmetric modes are reported in Table 3. A more detailed description of the Hamiltonian and the value of the parameters are reported in the ESI†.

Table 1 Linear intrastate coupling constant $\kappa^{(\alpha)}_i$ values (in eV) obtained in this work. The values between parenthesis are the dimensionless quantities $\kappa^{(\alpha)}_i/\omega_i$.

	$B_{3u}(n\pi^*)$	$A_u(n\pi^*)$	$B_{2u}(\pi\pi^*)$
κ_{6a}	-0.075(-1.021)	-0.162(-2.204)	0.136(1.851)
κ_1	-0.045(-0.357)	-0.088(-0.698)	-0.190(-1.506)
κ_{9a}	0.120(0.779)	-0.064(-0.416)	0.051(0.331)
κ_{8a}	-0.067(-0.337)	-0.413(-2.057)	0.056(0.281)

The adiabatic potential energy surfaces are obtained by diagonalizing the diabatic potential energy matrix $\boldsymbol{W}(\boldsymbol{Q})$, and the parameters of the model can be fitted to the adiabatic electronic energies computed using *ab-initio* electronic structure calculations. The methodology used for the electronic structure calculations has been presented in our previous work.[35] The aug-cc-pVDZ basis set of Dunning[82] was used in all the calculations. The ground state equilibrium geometry and vibrational modes were performed with the second-order Møller-Plesset (MP2) method, using the Gaussian 03 program package.[83] Excited state calculations were performed with the CASSCF and XMCQDPT2 method,[79] as implemented in the Firefly QC package,[84] which is partially based on the GAMESS (US) source code.[85] For the CASSCF wavefunction, an active space of ten electrons in eight orbitals, including the three occupied π orbitals, the three virtual π^* orbitals and the two nitrogen lone pair orbitals, was used. The orbitals were averaged over the five lowest CASSCF states (SA5-CASSCF). The XMCQDPT2 method is a new variant of multistate multireference perturbation theory especially designed for a correct description of excited states around avoided crossings and conical intersections. It has been applied to a number of problems of biological and photochemical interest,[86–93] and was shown to compare favorably with respect to experimental observations and other high-level theoretical methods.[94–97]

A detailed discussion and comparison of our XMCQDPT2 vertical excitation energies with respect to previously reported high-level *ab-initio* calculations can be found in our previous work.[35] Here we discuss our results in relation with the recent work of Fujimura *et al.*[36], in which the internal conversion to the $A_u(n\pi^*)$ state found in previous TSH dynamics simulations[52,54] and in our previous work[35] was claimed to be a consequence of the inaccuracy of the TDDFT and XMCQDPT2 methods. The authors used MRCI electronic structure calculations to construct various two-dimensional coupled diabatic potential energy surfaces and performed wavepacket propagations. They found no evidence of internal conversion from the initially excited $B_{2u}(\pi\pi^*)$ state to the $A_u(n\pi^*)$ state. Our XMCQDPT2 vertical excitation energies for the three lowest singlet excited electronic states are reported in Table 2 in comparison with the MRCI values of Fujimura *et al.*[36] and available experimental values.

The central issue at the origin of the discrepancy between the results of Fjimura *et al.* and ours is the relative position of the $A_u(n\pi^*)$ and $B_{2u}(\pi\pi^*)$ states, which remains controversial, despite the large amount of previous work devoted the characterization of the excited electronic states of pyrazine at its ground state equilibrium geometry.[20–27] The absorption band maximum of the $B_{2u}(\pi\pi^*)$ state has been measured at 4.81 eV.[10,11,16] It is well known, however, that the the absorption band maximum of a given state can differ from its vertical excitation energy.[98,99] The position of the $A_u(n\pi^*)$ state has been measured at 5.0 eV by near-threshold electron en-

Table 2 Experimental and calculated electronic excitation energies in eV. The value between parenthesis refers to the vertical excitation energy of the $A_u(n\pi^*)$ state adjusted to obtain the best agreement between our computed absorption spectrum and the experimental one.

	MRCI[36]	XMCQDPT2 (this work)	exp.
$B_{3u}(n\pi^*)$	4.55	3.93	3.83[a] [10]
$A_u(n\pi^*)$	5.52	4.45 (4.80)	5.0 [15]
$B_{2u}(\pi\pi^*)$	5.16	4.79	4.81 [10]

[a] 0-0 transition

ergy loss spectroscopy,[15]. However, this value appears controversial. For instance, a value of 4.72 eV was considered in refs.[26,27] as a reference value.

From the theoretical point of view, rather large variations in the exist among the calculated relative energy of the $A_u(n\pi^*)$ and $B_{2u}(\pi\pi^*)$ states reported in the litterature (see Table 3 in ref.[35]). Briefly, previous CASPT2[22,24,27,100] and CC2[101] calculations predicted the $A_u(n\pi^*)$ state to lie below the $B_{2u}(\pi\pi^*)$ state. CC3 calculations[101] predicted these two states to be essentially degenerate, whereas SAC-CI[26], EOM-CCSD(T)[23] and MRCI[35] calculations predicted the $A_u(n\pi^*)$ state to lie above the $B_{2u}(\pi\pi^*)$ state. Note that the EOM-CCSD(T) calculations[23] predicted the $B_{2u}(\pi\pi^*)$ state vertical excitation energy at 4.64 eV, which is below the experimental 0-0 transition of 4.69 eV.[16]

As seen in Table 2, our XMCQDPT2 values for the bright $B_{3u}(n\pi^*)$ and $B_{2u}(\pi\pi^*)$ states are in good agreement with the experimental values. In contrast, as discussed in our previous work,[35] our vertical excitation energy for the dark $A_u(n\pi^*)$ state appears underestimated with respect to experiment. In order to cope with this issue, the $A_u(n\pi^*)$ state vertical excitation energy was adjusted to provide the best possible agreement between our calculated absorption spectrum and the experimental one (see Section 5.1). This strategy was also used in our previous work.[35] In this work, a value of 4.80 eV was retained. This value brings the $A_u(n\pi^*)$ and $B_{2u}(\pi\pi^*)$ states to near degeneracy at the FC geometry which is in reasonable agreement with experiment.

In contrast, the MRCI values of Fujimura *et al.* appear overestimated with respect to the experimental value. Specifically, their vertical excitation energy for the $B_{2u}(\pi\pi^*)$ state is 0.35 eV above the experimental value while the vertical excitation energies for the $B_{3u}(n\pi^*)$ and $A_u(n\pi^*)$ states appear too high by approximately 0.5 eV. Furthermore, in the work of Fujimura *et al.*, the possibility of an internal conversion process from the $B_{2u}(\pi\pi^*)$ state to the $A_u(n\pi^*)$ state was rejected on the basis of two-dimensional models. Specifically, two sets of two dimensional coupled diabatic PESs were constructed, including the ν_{6a} totally symmetric mode and the ν_4 mode of B_{2g} symmetry in the first case, and the ν_{6a} and the ν_5 mode of B_{2g} symmetry in the second case. We believe that such low dimensional model, while informative, are not sufficient to rule out the importance of the $A_u(n\pi)$ state in the excited state dynamics of pyrazine. First it is known that a qualitatively correct simulation of the absorption spectrum requires at least to take into account the ν_1 and ν_{9a} totally symmetric modes.[32,34] In addition, the ν_4 and ν_5 coupling modes should be taken into account together as their contribution to the coupling between the $B_{2u}(\pi\pi^*)$ and $A_u(n\pi^*)$ state adds up. To support our point, we have performed quantum dynamics simulations of the excited state dynamics of the molecule after excitation to the $B_{2u}(\pi\pi^*)$ state using our 10D model and two different values of 4.8 and 5.0 eV for the $A_u(n\pi^*)$ state vertical excitation energy. These calculations, presented in the ESI†, show that even in the second case, where the $A_u(n\pi^*)$ state lies 0.21 eV above the $B_{2u}(\pi\pi^*)$ state at the FC geometry, a significant amount of population is transfered to the $A_u(n\pi^*)$ state during the first 100 fs after excitation.

We thus believe that, provided that the adjusted value for the $A_u(n\pi^*)$ state vertical excitation energy is used in our model, the internal conversion from the $B_{2u}(\pi\pi^*)$ state to the $A_u(n\pi^*)$ state observed in our quantum dynamics simulations is not an artefact caused by a lack of accuracy of our electronic structure calculations.

Our model includes 258 parameters, which were obtained by a least-square fit to more than 5000 XMCQDPT2 *ab-initio* points. In the fitting of large vibronic coupling model potentials,[98,102,103] it is customary to multiply the function to optimize by a weight function, in order to ensure a better accuracy of the model in low-energy regions of the nuclear configuration space. However, in our case, the conical intersection between the ground and $A_u(n\pi^*)$ states occur at rather high energies, see Fig. 5 in Section 3 below. Therefore, applying a weight function giving priority to low-energy geometries would have resulted in an inaccurate model potential in the region of this conical intersection, which is a key feature for the process investigated in this work. To avoid this problem, the

Table 3 Quadratic intrastate $\gamma_{ii}^{(\alpha)}$ and linear interstate coupling constant $\lambda_i^{(\alpha\alpha')}$ values (in eV) obtained in this work. The values between parenthesis are the dimensionless quantities $\lambda_i^{(\alpha\alpha')}/\omega_i$.

mode	symm.	λ	$\gamma^{(1)}$	$\gamma^{(2)}$	$\gamma^{(3)}$	$\gamma^{(4)}$
ν_{10a}	B_{1g}	0.190(1.638)	0.008	-0.016	-0.046	-0.010
ν_4	B_{2g}	0.062(0.682)	-0.007	-0.032	-0.031	-0.032
ν_5	B_{2g}	0.031(0.266)	-0.002	-0.017	-0.029	-0.021
ν_{8b}	B_{3g}	0.205(1.065)	0.045	-0.011	0.002	-0.015
ν_{16a}	A_u	0.152(3.638)	0.003	0.012	-0.009	-0.028
ν_{17a}	A_u	0.134(1.119)	0.001	-0.020	-0.040	-0.025

calculated points were separated in two groups. A first group, denoted G_1, containing points calculated at geometries around the Franck-Condon region, where the weight function was applied, and a second group, denoted G_2, containing points calculated at geometries around the conical intersection between the ground and $A_u(n\pi^*)$ states and the pathway connecting it to the Franck-Condon region, where the weight function was not applied. The functional to be optimized was thus expressed as

$$\Delta = \sum_{\alpha}\sum_{i\in G_1}\left(V_i^{(\alpha)} - V_i^{(\alpha),\mathrm{mod}}\right)^2 F_i^{(\alpha)} + \sum_{\alpha}\sum_{j\in G_2}\left(V_j^{(\alpha)} - V_j^{(\alpha),\mathrm{mod}}\right)^2. \quad (7)$$

In this equation, the weight function is given by

$$F_i^{(\alpha)} = \exp\left[-\left(V_i^{(\alpha)} - V_0^{(\alpha)}\right)\right], \quad (8)$$

where $V_0^{(\alpha)}$ is the value of the α^{th} adiabatic potential at the ground state equilibrium geometry. The optimization was performed using a pseudo-Newton-Raphson method with approximate Hessian updated through the Broyden-Fletcher-Goldfarb-Shanno scheme. A weighted root-mean-square deviation of 0.053 eV was achieved.

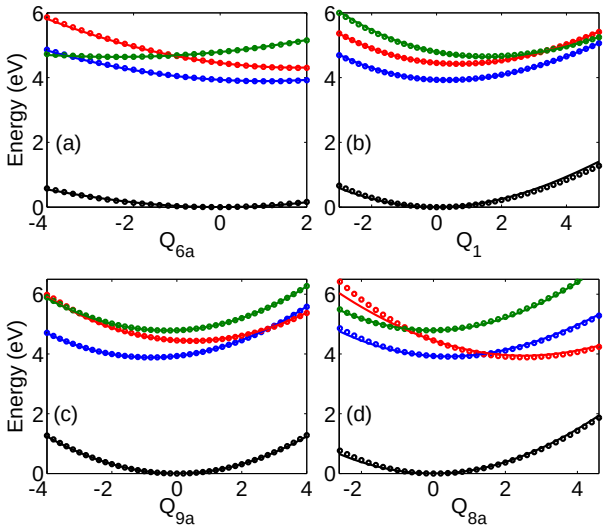

Fig. 1 Cuts of the potential energy surfaces of the ground (black), $B_{3u}(n\pi^*)$ (blue), $A_u(n\pi^*)$ (red) and $B_{2u}(\pi\pi^*)$ (green) states along the four totally symmetric dimensionless normal coordinates. The circles represent the XMCQDPT2 energies and the solid lines represent the energies obtained from our model potentials (see Section 2).

Cuts of the potential energy surfaces along the four totally symmetric modes included in our model are presented in Fig. 1. Both the *ab-initio* energies and the energies obtained from our model are shown. Fig. 1 (a) presents a cut along the ν_{6a} mode. It shows the existence of $A_u(n\pi^*)/B_{2u}(\pi\pi^*)$ and $B_{3u}(n\pi^*)/B_{2u}(\pi\pi^*)$ conical intersections lying close to the ground state equilibrium geometry, explaining the competition between internal conversion to the $B_{3u}(n\pi^*)$ and to the $A_u(n\pi^*)$ states, after excitation to the $B_{2u}(\pi\pi^*)$ state found in our previous work.[35] Fig. 1 (d) presents cuts of the potential energy surfaces along the ν_{8a} mode and shows the existence of a low-lying conical intersection between the $B_{3u}(n\pi^*)$ and $A_u(n\pi^*)$ states, which was found in our previous work[35] to be responsible for oscillations of the population between these two states after the initial decay from the $B_{2u}(\pi\pi^*)$ state.

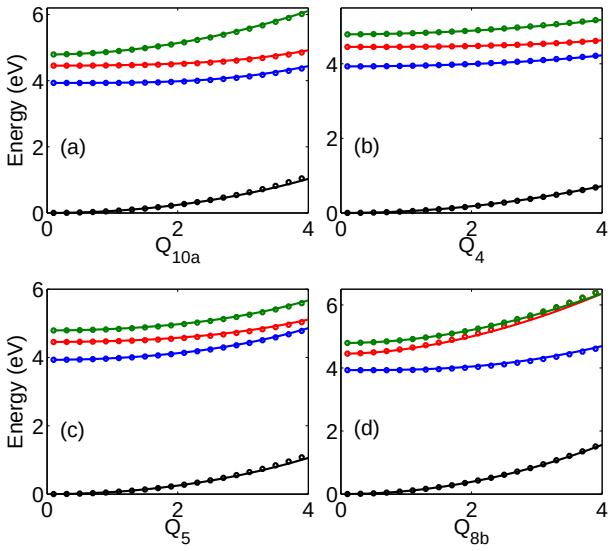

Fig. 2 Cuts of the potential energy surfaces of the ground (black), S_1 (blue), S_2 (red) and S_3 (green) states along the non-totally symmetric dimensionless normal coordinates Q_{10a}, Q_4, Q_5 and Q_{8b}. The circles represent the XMCQDPT2 energies and the solid lines represent the energies obtained from our model potentials (see Section 2).

Cuts of the potential energy surfaces along the B_{1g} ν_{10a} mode, the B_{2g} ν_4 and ν_5 modes and the B_{3g} ν_{8b} mode are presented in Fig. 2. As seen in Table 3, the linear interstate coupling constants associated with the ν_{10a} mode, which couples the $B_{3u}(n\pi^*)$ and $B_{2u}(\pi\pi^*)$ states at first order, and with the ν_{8b} mode, which couples the $B_{3u}(n\pi^*)$ and $A_u(n\pi^*)$ states at first order, are large. These strong couplings result in a repelling of the corresponding adiabatic potential energy surfaces, as seen in Fig. 2 (a) and (d). The coupling between the $A_u(n\pi^*)$ and $B_{2u}(\pi\pi^*)$ states, mediated by the ν_4 and ν_5 modes is comparatively smaller, as seen in table 3 and Fig. 2 (b) and (c).

3 Decay pathways to the ground electronic state

After the initial ultrafast decay from the $B_{2u}(\pi\pi^*)$ state, pyrazine further decays to its ground electronic state on a much longer time scale of approximately 20 ps.[17,18] This decay process has been interpreted in light of the theoretical work of Domcke *et al.*[64] who reported the existence of a conical intersection between the $A''(\pi\pi^*)$ excited state and the ground state at a geometry which is reminiscent of the prefulvene conical intersection in benzene.[65–73] We note that similar conical intersections have been reported for other simple benzene derivatives such as phenol[104] or aniline.[105] In all these molecules, the prefulvene conical intersection is separated from the Franck-Condon region by a potential energy barrier. The geometries of the minimum and prefulvene transition state on the $A''(\pi\pi^*)$ state were optimized at the state specific CASSCF level of theory. The prefulvene minimum energy conical intersection with the ground state was optimized at the state averaged CASSCF level of theory with equal weights given to the two states forming the conical intersection. These geometries are shown in Fig. 3.

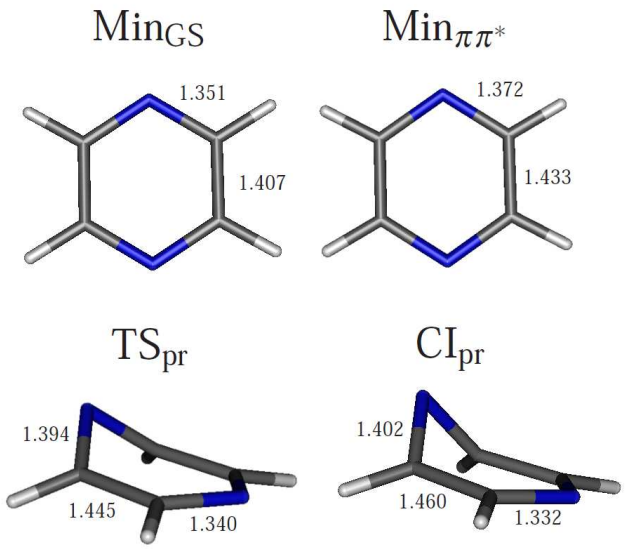

Fig. 3 Ground state equilibrium geometry (Min$_{GS}$) optimized at the MP2 level of theory and $B_{2u}(\pi\pi^*)$ state minimum (Min$_{\pi\pi^*}$) prefulvene transition state (TS$_{pr}$) and prefulvene minimum energy conical intersection (CI$_{pr}$) geometries optimized at the CASSCF level of theory. The nitrogen atoms are featured in blue, the carbon atoms in gray and the hydrogen atoms in white. The CN and CC bond lengths are given in Å.

The $B_{2u}(\pi\pi^*)$ minimum has a D_{2h} geometry with elongated CC and CN bonds, with respect to the ground state equilibrium geometry. The prefulvene transition state and minimum energy conical intersection have a C_s symmetry, and are characterized by an out-of-plane distortion of one of the two nitrogen atoms of the molecule. They both show an elongation of the CC bonds and of the CN bonds involving the out-of-plane nitrogen atom, and a contraction of the other CN bonds. We computed a linearly interpolated scan in internal coordinates (LIIC), at the SA5-CASSCF and XMCQDPT2 levels of theory, between the minimum of the $B_{2u}(\pi\pi^*)$ state and the prefulvene conical intersection. These scans were split into two parts, a first part between the minimum of the $B_{2u}(\pi\pi^*)$ state and the prefulvene TS, and a second part between the prefulvene TS and the prefulvene MECI. The results of these calculations are presented in Fig. 4. At the CASSCF level

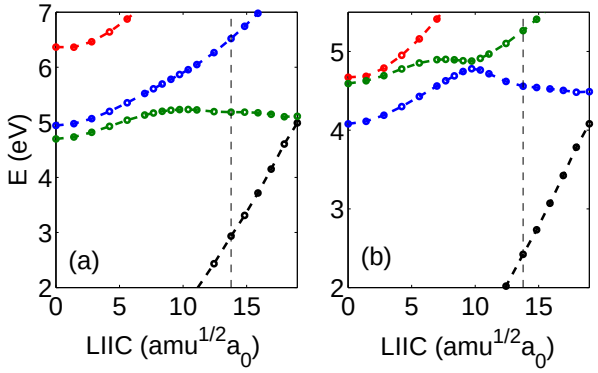

Fig. 4 Linearly interpolated scans from the minimum of the $B_{2u}(\pi\pi^*)$ state to the prefulvene minimum energy conical intersection through the transition state (see text for details), computed at the SA5-CASSCF (a) and XMCQDPT2 (b) levels of theory. The vertical black dashed line show the position of the SS-CASSCF optimized prefulvene transition state. The potential energy scans corresponding to the adiabatic electronic states continuously connected to the ground state (black), $B_{3u}(n\pi^*)$ state (blue), $A_u(n\pi^*)$ state (red) and $B_{2u}(\pi\pi^*)$ state (green), at D_{2h} symmetry, are shown. The dashed lines connecting the points are plotted to guide the eyes.

of theory (panel (a) of Fig. 4), the $B_{2u}(\pi\pi^*)$ state is the first excited state at its minimum geometry, with an energy of 4.70 eV with respect to the ground state equilibrium geometry. The CASSCF LIIC shows the existence of a rather large potential energy barrier of approximately 0.54 eV on the pathway leading to the prefulvene conical intersection. One can see in this figure that the TS on the $A''(\pi\pi^*)$ curve does not match the position of the optimized TS, given by the vertical black dashed line. This is because the optimization was performed at the SS-CASSCF level of theory whereas the potential energy scan was performed at the SA5-CASSCF level of theory. The XMCQDPT2 LIIC (panel (b) of Fig. 4) shows rather different energies and topographies of the potential energy curves. This indicates that the inclusion of the dynamic electronic cor-

relation effects is necessary to obtain accurate results. At the XMCQDPT2 level of theory, the $B_{2u}(\pi\pi^*)$ state is the second excited state at its minimum geometry, above the $B_{3u}(n\pi^*)$ state, with an energy of 4.59 eV with respect to the ground state equilibrium geometry. In addition, while at the CASSCF level of theory, the $A_u(n\pi^*)$ state is much higher in energy, at the XMCQDPT2 level of theory, it lies only slightly above the $B_{2u}(\pi\pi^*)$ state. The XMCQDPT2 LIIC shows the existence of a potential energy barrier of approximately 0.30 eV, significantly smaller than the CASSCF barrier. The $A''(n\pi^*)$ and $A''(\pi\pi^*)$ states (the adiabatic states continuously connected to the $B_{3u}(n\pi^*)$ and $B_{2u}(\pi\pi^*)$ states) form a narrowly avoided crossing just after the barrier, because at C_s geometries, both states have A'' symmetry.

It is well known that the benzene molecule shows a similar decay pathway involving a prefulvene conical intersection between the first $\pi\pi^*$ excited state and the ground state, separated from the Franck-Condon geometry by a potential energy barrier.[64,65] Experimentally, after excitation close to the origin of the first $\pi\pi^*$ state, no ultrafast dynamics is observed, and the molecule decays *via* fluorescence and intersystem crossing. However, after excitation to the first $\pi\pi^*$ excited state with an excess energy of more than 3000 cm^{-1}, an ultrafast decay on a time scale of the order of 200 fs is observed.[70,72] This excess energy is interpreted as the energy needed to overcome the potential energy barrier along the prefulvene pathway. By analogy, the prefulvene decay channel in pyrazine is not expected to be open below approximately 4.9 eV, which is our estimated energy at the top of the potential energy barrier on the $A''(\pi\pi^*)$ state. Therefore, the decay to the ground state observed experimentally with a time constant of approximately 20 ps after excitation at a wavelength of 266.7 nm ($\sim$ 4.65 eV) should proceed *via* a different mechanism.

In this paper, we propose an alternative mechanism to explain the decay of pyrazine to its ground electronic state. It involves a conical intersection between the $A_u(n\pi^*)$ state, populated almost immediately after excitation to the $B_{2u}(\pi\pi^*)$ state, and the ground state. Fig. 5 presents cuts of the potential energy surfaces of the four electronic states of interest along an effective coordinate defined as $Q_{\text{eff}} = \kappa_{6a}Q_{6a} + \kappa_1 Q_1 + \kappa_{8a}Q_{8a} + \kappa_{9a}Q_{9a}$, where the κ_i are the components of the gradient of the $A_u(n\pi^*)$ potential energy surface at the ground state equilibrium geometry along the totally symmetric modes obtained in our previous work.[35] It shows the existence of a conical intersection between the $A_u(n\pi^*)$ state and the ground state. This conical intersection appears rather high in energy. However, we note that the crossing point shown in Fig. 5 is not the minimum of the seam of conical intersection between the $A_u(n\pi^*)$ state and the ground state. In addition, even if, after excitation at approximately 4.65 eV, the wavepacket does not have a sufficient energy to reach the actual seam of conical intersection, it can reach a region where the $A_u(n\pi^*)$ and the

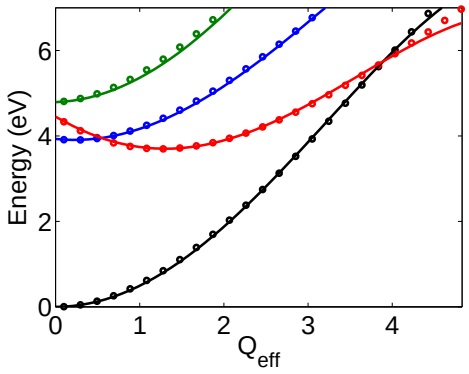

Fig. 5 Cut of the potential energy surfaces of the ground (black) $B_{3u}(n\pi^*)$ (blue), $A_u(n\pi^*)$ (red) and $B_{2u}(\pi\pi^*)$ (green) states along an effective coordinate Q_{eff}. The circles represent the XMCQDPT2 energies and the solid line represent the energies obtained from our model potentials (see Section 2).

ground state potential energy surfaces are close in energy, and where a slow internal conversion to the ground state can occur, consistently with the large time constant of approximately 22 ps observed experimentally.[17,18] In addition, as seen in Table 3, the linear interstate coupling constant associated with the A_u ν_{16a} and ν_{17a} modes, which couple the ground and $A_u(n\pi^*)$ states at first order, are rather large. We note that, although these two coupling constants have similar values, because the frequency of the ν_{16a} mode is significantly lower than the frequency of the ν_{17a} mode (our MP2 computed values are $\omega_{16a} = 337$ cm^{-1} and $\omega_{17a} = 942$ cm^{-1}, see Table 2 in ref.[35]), the coupling between the ground and $A_u(n\pi^*)$ states is expected to be predominantly mediated by the ν_{16a} mode. In Fig. 6, we present cuts of the potential energy surfaces of the adiabatic electronic states continuously connected to the ground and $A_u(n\pi^*)$ state at D_{2h} symmetry along the two A_u ν_{16a} and ν_{17a} modes for different fixed values of Q_{eff}. Here, the model potentials reproduce slightly less accurately the *ab-initio* points than in Figs. 1 and 2, because the potential cuts presented in Fig. 6 correspond to geometries involving significant displacements along five coordinates. The effect of the vibronic coupling on the shape of the adiabatic potential energy curves is seen, even at geometries where the two coupled electronic state are separated by a significant energy gap. This is the case, for instance, in panel (c) of Fig. 6, showing cuts of the potentials along the ν_{16a} mode at a fixed value of $Q_{\text{eff}} = 2.85$. The energy difference between the two adiabatic states is of roughly 1 eV at $Q_{16a} = 0$, and yet, the potential energy curves show an avoided crossing, characteristic of a significant non-adiabatic coupling.

We note here that the model Hamiltonian presented in Section 2 is not able to describe the prefulvene decay pathway

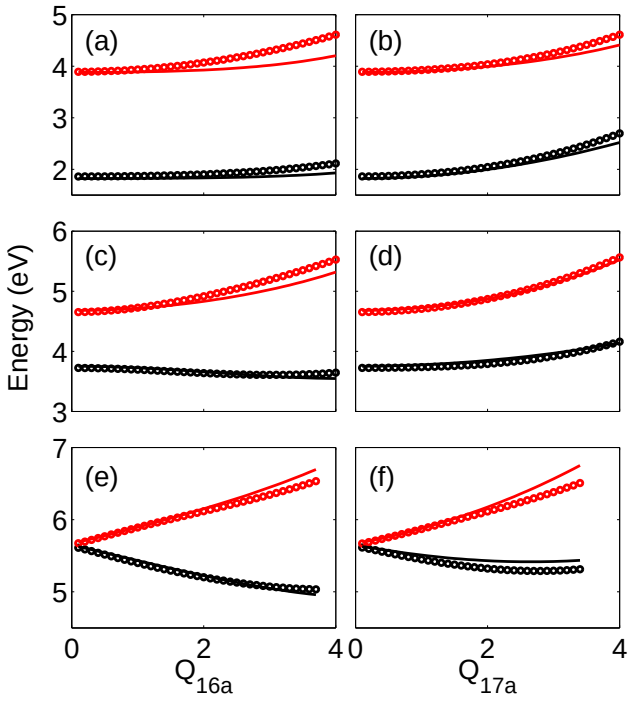

Fig. 6 Cut of the potential energy surfaces of the ground (black) and $A_u(n\pi^*)$ (red) states along the Q_{16a} and Q_{17a} coordinates for different values of the effective coordinate $Q_{\rm eff}$ (see Fig. 5), $Q_{\rm eff} = 1.87$ (a) and (b), $Q_{\rm eff} = 2.85$ (c) and (d), $Q_{\rm eff} = 3.74$ (e) and (f). The circles represent the XMCQDPT2 energies and the solid line represent the energies obtained from our model potentials (see Section 2).

illustrated in Fig. 4. Because of its complicated topography, the description of this region of the potential energy surfaces would require a more sophisticated model, as was shown in the case of benzene.[71] In addition, the prefulvene pathway leading to a conical intersection between the ground state and the adiabatic state connected with the $B_{2u}(\pi\pi^*)$ state, the inclusion of the vibrational modes mediating the corresponding vibronic coupling would have been required. Because we do not describe the prefulvene pathway, in our model, the ground state is well separated from both the $B_{3u}(n\pi^*)$ and $B_{2u}(\pi\pi^*)$ states. This allows us to neglect the B_{3u} and B_{2u} modes, mediating the corresponding vibronic couplings at first order.

A second important comment concerns the inclusion of high order terms in our model. Our aim is to describe the dynamics of the molecule after the initial ultrafast internal conversion process occurring on the bright $B_{2u}(\pi\pi^*)$ state. In our previous work, we have found that, because of the existence of conical intersections between the $B_{2u}(\pi\pi^*)$ state and both the $A_u(n\pi^*)$ and $B_{3u}(n\pi^*)$ states, lying close to the Franck-Condon geometry (see Fig. 1 (a)), this internal conversion process transfers population to both the $A_u(n\pi^*)$ and $B_{3u}(n\pi^*)$ states. During this process, one expects a significant excitation of the coupling modes associated with these two conical intersections, which are the B_{2g} and B_{1g} modes respectively. In addition, the wavepacket is expected to show rather large amplitude motions along the totally symmetric modes because of the large first order intrastate coupling constants (see Table 1). Finally, because the internal conversion process to the ground state observed experimentally[17,18] is a slow process, we need to describe the dynamics of the molecule for a relatively long time. One can thus expect the wavepacket to explore rather extended regions of the potential energy surfaces during the dynamics, which is the reason why it was necessary to include high-order terms in our model, in order to ensure a sufficient accuracy, not only in the Franck-Condon region. The model derived in this paper therefore allows us to assess the ability of the alternative decay mechanism described above to account for the internal conversion to the ground state observed experimentally,[17,18] see Section 5 below.

4 The multi-configuration time-dependent Hartree method

The nuclear time-dependent Schrödinger equation associated with the model Hamiltonian presented in Section 2 was solved using the multi-configuration MCTDH method[74–77] as implemented in the Heidelberg MCTDH package.[106] The MCTDH ansatz for the wavefunction reads

$$|\Psi\rangle = \sum_{\alpha=1}^{n_\alpha} \Psi^{(\alpha)}(\boldsymbol{Q},t)|\alpha\rangle, \tag{9}$$

where $\{|\alpha\rangle\}$ denotes the set of diabatic electronic states. The nuclear wavefunction $\Psi^{(\alpha)}(\boldsymbol{Q},t)$ in the electronic state $|\alpha\rangle$ is expanded in a basis of multi-dimensional time-dependent functions $\varphi(q_\kappa,t)$ called single-particle functions (SPFs)

$$\begin{aligned}\Psi^{(\alpha)}(\boldsymbol{Q},t) &\equiv \Psi^{(\alpha)}(\boldsymbol{q},t)\\ &= \sum_{j_1^{(\alpha)}}^{n_1^{(\alpha)}} \cdots \sum_{j_p^{(\alpha)}}^{n_p^{(\alpha)}} A^{(\alpha)}_{j_1,\cdots,j_p} \prod_{\kappa=1}^{p} \varphi^{(\kappa,\alpha)}_{j_\kappa^{(\alpha)}}(q_\kappa,t).\end{aligned} \tag{10}$$

The coordinate q_κ is a collective coordinate $q_\kappa = (Q_{1,\kappa},...,Q_{d,\kappa})$, also called combined mode. The SPFs are expanded in a primitive basis, built as a direct product of one-dimensional basis functions for each degree of freedom

$$\varphi^{(\kappa)}_{j_\kappa}(q_\kappa,t) = \sum_{l_1}^{N_{1,\kappa}} \cdots \sum_{l_d}^{N_{d,\kappa}} a_{j_\kappa,l_1\ldots l_d} \chi^{(\kappa)}_{l_1}(Q_{1,\kappa})\cdots\chi^{(\kappa)}_{l_d}(Q_{d,\kappa}). \tag{11}$$

The equations of motion for the expansion coefficients and for the SPFs are derived variationally, which ensures an optimal

Table 4 Number of SPF and primitive basis functions used in the calculations.

Combinations of modes	SPF basis 1	SPF basis 2	Numbers of grid points
(ν_{6a}, ν_{8a})	[40,34,41,26]	[42,38,46,30]	(48,36)
$\nu_{10a}, \nu_{16a})$	[31,36,40,29]	[32,38,44,32]	(22,29)
$(\nu_4, \nu_5, \nu_{17a})$	[25,30,40,22]	[26,32,44,24]	(19,11,15)
$(\nu_1, \nu_{9a}, \nu_{8b})$	[42,38,47,27]	[44,42,50,30]	(32,16,15)

description of the wavepacket with a SPF basis of reasonable size.

The MCTDH method is a general method for the solution of the time-dependent Schrödinger equation for high-dimensional quantum systems. Beyond problems of photochemical interest,[107–109] the MCTDH method has been recently applied to a broad range of problems in topics such as intramolecular vibrational energy redistribution,[110–112] infrared spectroscopy,[113,114] reactive scattering,[115] laser control of unimolecular processes,[116,117] or attosecond spectroscopy.[118]

In this work, for the representation of the Hamiltonian and the wavefunction, a Hermite polynomial DVR scheme[119] was used for all the degrees of freedom. The number of SPF and primitive basis functions used in the calculations are listed in Table 4.

5 Results and discussion

5.1 Simulation of the UV absorption spectrum

We have first simulated the UV absorption spectrum of the molecule in the region between 3.8 and 5.7 eV, corresponding to the two lowest absorption bands, using the model Hamiltonian presented in Section 2. In the time-dependent framework, the absorption cross-section at a photon energy E is computed as the Fourier transform of the autocorrelation function $a(t)$

$$\begin{aligned} S(E) &\propto E\int_{-\infty}^{\infty} a(t)e^{i(E+E_i)t}dt \\ &\propto 2E\int_{0}^{\infty} \mathrm{Re}\left[a(t)e^{i(E+E_i)t}\right]dt, \end{aligned} \qquad (12)$$

with $a(t) = \langle\Psi(\boldsymbol{Q},0)|\Psi(\boldsymbol{Q},t)\rangle$. To account for the homogeneous broadening of the experimental spectrum, the autocorrelation function was pre-multiplied by a damping function $f(t) = e^{-t/\tau}$. This is equivalent to convoluting the spectrum by a Lorentzian function of full width at half maximum of $2/\tau$. In addition, to avoid problems arising from the finite propagation time T, the autocorrelation function was further pre-multiplied by a filter function $g(t) = \cos(\pi t/2T)\Theta(t-T)$, where Θ denotes the Heaviside step function.

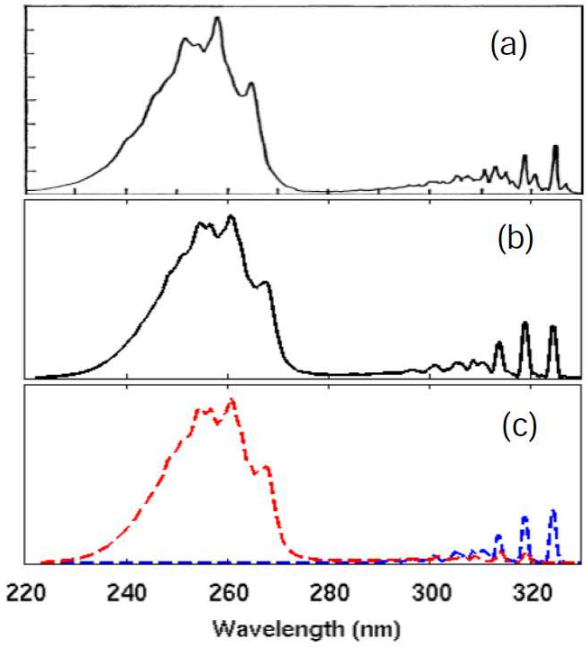

Fig. 7 Absorption spectrum obtained in this work, compared with the experimental spectrum.[10] Panel (b) shows the full spectrum and panel(c) shows the $B_{3u}(n\pi^*)$ (blue) and $B_{2u}(\pi\pi^*)$ (red) partial spectra.

The two lowest bands in the UV absorption spectrum are dominated by transitions to the bright $B_{3u}(n\pi^*)$ and $B_{2u}(\pi\pi^*)$ states. The transition from the ground state to the $A_u(n\pi^*)$ state is forbidden by symmetry at the D_{2h} equilibrium geometry. Two wavepacket propagations were performed, starting on the $B_{3u}(n\pi^*)$ and $B_{2u}(\pi\pi^*)$ states respectively, from which two partial absorption spectra were computed. In each case, a vertical excitation was assumed, *i.e* the initial wavefunction was obtained as the ground vibronic state wavefunction projected in each diabatic excited electronic state. The full absorption spectrum was then computed as the oscillator strength-weighted sum of the two partial absorption spectra. The experimental estimations of 0.006 and 0.1 for the oscillator strengths of the $B_{3u}(n\pi^*)$ and $B_{2u}(\pi\pi^*)$ states re-

spectively,[13] were used. Each partial absorption spectrum was computed from a propagation of 120 fs. Damping times τ of 400 fs and 100 fs were used for the $B_{3u}(n\pi^*)$ and $B_{2u}(\pi\pi^*)$ components, respectively. The whole computed spectrum was blue-shifted by 0.16 eV so that the position of the $B_{3u}(n\pi^*)$ 0-0 peak matches the experimental one at approximately 324 nm. In addition, as in our previous work,[35] the vertical excitation energy of the $A_u(n\pi^*)$ state was adjusted to improve the agreement between the computed and experimental spectra. A value of 4.80 eV was found to provide the most satisfactory agreement (see the discussion in 2). Our computed spectrum, in comparison with experiment,[10] is presented in Fig. 7. We obtained an excellent agreement with the experimental spectrum for the broad band between 270 and 220 nm corresponding to a transition to the $B_{2u}(\pi\pi^*)$ state. In contrast, the agreement is more qualitative for the lower band between 330 and 300 nm corresponding to a transition to the $B_{2u}(\pi\pi^*)$ state. Overall, our spectrum is of similar quality than the spectrum obtained in our previous work using a simpler linear vibronic coupling Hamiltonian augmented with diagonal quadratic terms.[35] By taking into account the overall energy shift and the adjustment of the $A_u(n\pi^*)$ state vertical excitation energy applied in our model, we propose refined estimations of 4.09, 4.96 and 4.95 eV for the vertical excitation energies of the $B_{3u}(n\pi^*)$, $A_u(n\pi^*)$ and $B_{2u}(\pi\pi^*)$ states, respectively.

5.2 Electronic state population dynamics

In this Section, we present simulations of the dynamics of the molecule after photoexcitation to the $B_{2u}(\pi\pi^*)$ state using the model Hamiltonian presented in Section 2. In order to get as close as possible to the experimental conditions,[18] the photoexcitation was modelized by the explicit inclusion of the interaction of the molecule with a 130 fs laser pulse. Specifically, the total Hamiltonian reads

$$\boldsymbol{H}(\boldsymbol{Q},t) = \boldsymbol{H_0}(\boldsymbol{Q}) + \boldsymbol{H}_{int}(t), \tag{13}$$

where $\boldsymbol{H_0}(\boldsymbol{Q})$ is the diabatic Hamiltonian of eq. (1), and $\boldsymbol{H}_{int}(t)$ is the operator describing the interaction of the molecule with the laser field in the dipolar approximation. Simulations with laser pulse photon energies of 4.65 and 4.75 eV were performed. As in Sec. 5.1, the Franck-Condon approximation was used. Tests calculations including Hetzberg-Teller terms in the dipole moments were performed and found to provide results extremely similar to those obtained using the Franck-Condon approximation. As explained in Section 3, our aim was to describe the slow decay of the molecule to its ground state after the initial ultrafast decay from the bright $B_{2u}(\pi\pi^*)$ state. This implies the propagation of a highly vibrationally excited wavepacket for a relatively long time. Therefore, large primitive and SPF bases were necessary to reach a satisfactory level of convergence. Details of the bases used in our calculations are given in Table 4. Two different SPF bases, denoted SPF basis 1 and SPF basis 2, were used for the calculations with excitation photon energies of 4.65 and 4.75 eV, in order to reach a similar level of convergence in the two calculations. A larger SPF basis was needed in the second case since it involves a wavepacket with a greater amount of internal energy. The calculation with the SPF basis 1 involved approximately 6.2×10^6 configurations and the calculation with the SPF basis 2 approximately 8.6×10^6 configurations. For comparison, the largest calculation for the full dimensional two-state model presented in ref.[40] involved approximately 2.8×10^6 configurations, while a larger calculation has been reported on the same model,[41] including approximately 4.6×10^7 configurations. The diabatic electronic state populations obtained for 1 ps propagations are presented in Fig. 8. In both cases, almost immediately after excitation to the bright $B_{2u}(\pi\pi^*)$ state, the population decays to both the $B_{3u}(n\pi^*)$ and the $A_u(n\pi^*)$ states, in agreement with previous TSH nonadiabatic dynamics simulations.[52,54] This is in contrast to the previously accepted picture of the ultrafast rediationless decay of photoexcited pyrazine, involving an internal conversion at the conical intersection between the $B_{2u}(\pi\pi^*)$ and $B_{3u}(n\pi^*)$ states.[19,28–34,36–42] As seen in Fig. 1 (a), besides the conical intersection between the $B_{2u}(\pi\pi^*)$ and $B_{3u}(n\pi^*)$ states, a conical intersection between the $B_{2u}(\pi\pi^*)$ and $A_u(n\pi^*)$ states also exists in the Franck-Condon region, explaining the competition between the internal conversion to the $B_{3u}(n\pi^*)$ state and the internal conversion to the $A_u(n\pi^*)$ state. This feature of the excited state dynamics of pyrazine due to the existence of the dark $A_u(n\pi^*)$ state has been described in our previous work.[35] The population of the $B_{3u}(n\pi^*)$ state reaches a maximum at approximately $t = 140$ fs and then a slow internal conversion process, transferring population from the $B_{3u}(n\pi^*)$ state to the $A_u(n\pi^*)$ state is observed. This internal conversion process is explained by the existence of a low-lying conical intersection between the $B_{3u}(n\pi^*)$ and $A_u(n\pi^*)$ states, as can be seen in Figs. 1 (d) and 5. In the same time, a slow decay to the ground state is observed (see Fig. 8 panels (b) and (d)), which is consistent with the existence of a rather high-lying conical intersection between the $A_u(n\pi^*)$ and the ground state, as seen in Fig. 5. Experimentally, Stert *et al.* measured exponential decay time constants of 22 ps and 17.5 ps corresponding to a decay to the ground electronic state after excitation using pump photon energies of 4.65 and 4.75 eV respectively.[18] These time scales imply a nearly complete decay of the population after more than 100 ps (see Fig. 5 in ref.[18]). Our results are in good qualitative agreement with these experimental results. Our calculations predict a transfer of no more than 2 % of the population 1 ps after the excitation, implying a decay process occurring in a time scale of several tens of picoseconds. In addition, a slightly larger decay rate is predicted after

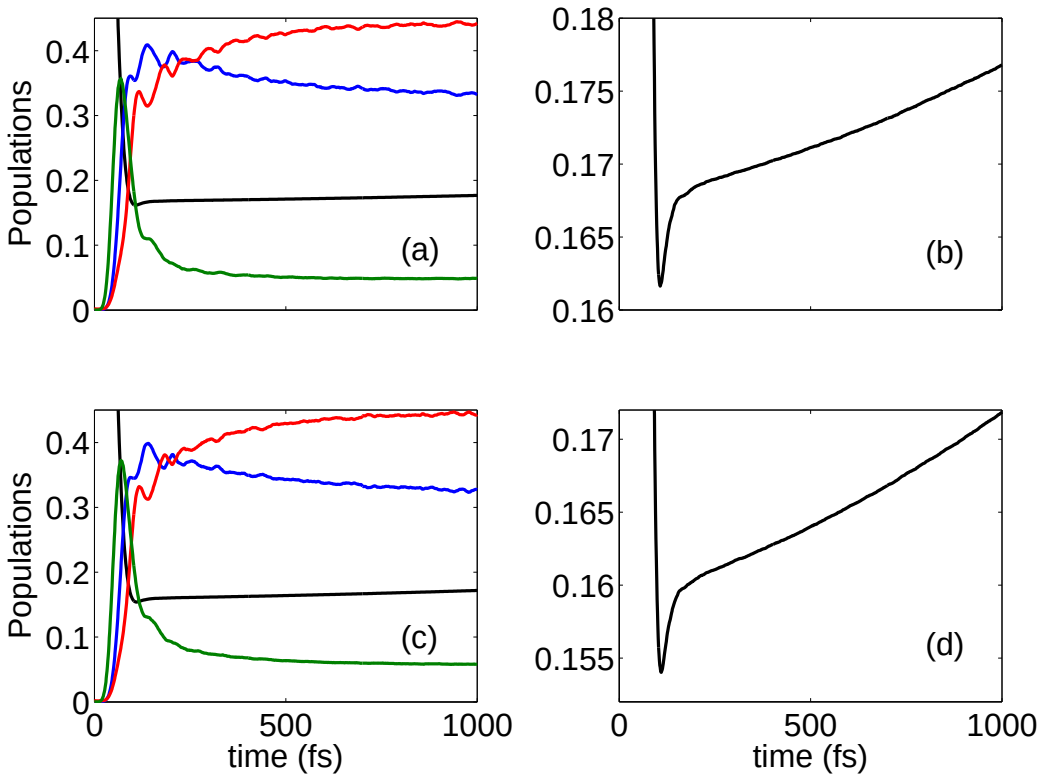

Fig. 8 Diabatic electronic state populations for the molecule excited by a 130 fs pulse of peak amplitude $A_0 = 0.004$ a.u, corresponding to a peak intensity $I \approx 0.56$ TW/cm^2. Panels (a) and (c) show the populations of the ground (black), $B_{3u}(n\pi^*)$ (blue), $A_u(n\pi^*)$ (red) and $B_{2u}(\pi\pi^*)$ (green) states for pulse photon energies of 4.65 and 4.75 eV, respectively. Panels (b) and (d) show the ground state populations only, extracted from the same calculations.

excitation with a pump photo energy of 4.75 eV than after excitation with a pump photo energy of 4.65 eV. In the first case, only approximately 1.5 % of the population is transfered to the ground state after 1 ps, whereas in the second case, approximately 1.8 % of the population is transfered to the ground state after 1 ps. As explained in Section 3, our model is not able to describe the prefulvene decay pathway. Nevertheless, our results show that the alternative decay mechanism proposed in this work is able to account for the internal conversion process to the ground state observed experimentally [17,18] in a satisfactory way.

6 Conclusion

We have presented quantum dynamics simulations of the excited state dynamics of pyrazine triggered by a resonant femtosecond pulse, with a particular focus on the radiationless decay of the molecule back to its ground electronic state. We have first analyzed the possible decay mechanisms using CASSCF and XMCQDPT2 electronic structure calculations. The prefulvene decay pathway leading to a conical intersection between the bright $\pi\pi^*$ state and the ground state has previously been proposed to explain the decay of the molecule to its ground state. However we have found a substantial potential energy barrier along this pathway, which is not consistent with the decay observed experimentally after excitation at 266.7 and 261.3 nm.[18] We have proposed a previously unknown radiationless decay pathway involving a conical intersection between the dark $A_u(n\pi^*)$ state and the ground state occurring upon motion along an effective totally symmetric coordinate dominated by the Q_{8a} vibrational mode. This decay mechanism appears more consistent with the experimental observations, and its ability to explain the radiationless decay to the ground state has been further checked using quantum dynamics calculations. We have constructed a quadratic vibronic coupling model augmented with selected third and fourth order terms, including the four lowest electronic states and ten vibrational modes. We have first computed the UV

absorption spectrum of the molecule in order to check the accuracy of our model and found a good agreement with the experimental spectrum. We have then simulated the dynamics of the molecule triggered by femtosecond laser pulses with photon energies of 4.65 and 4.75 eV. Consistently with previous TSH simulations[52,54] and with our previous work,[35] we have found an ultrafast decay of the population from the initially excited $B_{2u}(\pi\pi^*)$ state to both the $B_{3u}(n\pi^*)$ and the $A_u(n\pi^*)$ states. Subsequently, a slow internal conversion process to the ground state, occurring at the conical intersection between the $A_u(n\pi^*)$ state and the ground state, has been found. This internal conversion process is in good qualitative agreement with the experimental observations. Therefore, our calculations provide a significant new mechanistic insight into the photostability of pyrazine. In addition, they confirm the important role of the dark $A_u(n\pi^*)$ state in the photochemistry of the molecule. We hope that the results presented in this paper will stimulate further experimental efforts aiming at a direct observation of the participation of the dark $A_u(n\pi^*)$ state in the excited state dynamics of pyrazine.

7 Acknowledgements

Numerous discussions with prof. Hans-Dieter Meyer are gratefully acknowledged. We acknowledge support from the CoConicS Project (ANR-13-BS08-0013-03). M. S. and S. G. acknowledge support from the Conseil Régional de Bourgogne. Part of the calculations were performed using HPC resources from DSI-CCUB (Université de Bourgogne).

References

1 W. Domcke, D. Yarkony and H. Köppel, *Conical Intersections: Electronic Structure, Dynamics & Spectroscopy*, World Scientific, 2004.
2 W. Domcke, D. Yarkony and H. Köppel, *Conical Intersections: Theory, Computation and Experiment*, World Scientific, 2011.
3 V. Blanchet, M. Z. Zgierski, T. Seideman and A. Stolow, *Nature*, 1999, **401**, 52.
4 A. Stolow, A. E. Bragg and D. M. Neumark, *Chem. Rev.*, 2004, **104**, 1719.
5 T. Suzuki, *Annu. Rev. Phys. Chem.*, 2006, **57**, 555.
6 M. H. Beck, A. Jäckle, G. A. Worth and H.-D. Meyer, *Phys. Rep.*, 2000, **324**, 1.
7 M. Ben-Nun, J. Quenneville and T. J. Martínez, *J. Phys. Chem. A*, 2000, **104**, 5161.
8 J. C. Tully, *J. Chem. Phys.*, 1990, **93**, 1061.
9 W. H. Miller, *J. Phys. Chem. A*, 2009, **113**, 1405.
10 I. Yamazaki, T. Murao, T. Yamanaka and K. Yoshihara, *Faraday Discuss. Chem. Soc.*, 1983, **75**, 395.
11 A. Bolovinos, P. Tsekeris, J. Philips, E. Pantos and G. Anditsopoulos, *J. Mol. Spectrosc.*, 1984, **103**, 240.
12 J. Kommandeur, W. A. Majewski, W. L. Meerts and D. W. Pratt, *Annu. Rev. Phys. Chem.*, 1987, **38**, 433.
13 K. K. Innes, I. G. Ross and W. R. Moomaw, *J. Mol. Spectrosc.*, 1988, **132**, 492.
14 Y. Okuzawa, M. Fufii and M. Ito, *Chem. Phys. Lett.*, 1990, **171**, 341.
15 I. C. Walker and M. H. Palmer, *Chem. Phys.*, 1991, **153**, 169.
16 M. Stener, P. Decleva, D. M. P. Holland and D. A. Shaw, *J. Phys. B: At. Mol. Opt. Phys.*, 2011, **44**, 075203.
17 L. Wang, H. Kohguchi and T. Suzuki, *Faraday Discuss.*, 1999, **113**, 37.
18 V. Stert, P. Farmanara and W. Radloff, *J. Chem. Phys.*, 2000, **112**, 4460.
19 Y.-I. Suzuki, T. Fuji, T. Horio and T. Suzuki, *J. Chem. Phys.*, 2010, **132**, 174302.
20 W. R. Wadt, W. A. G. III and T. H. Dunning Jr., *J. Chem. Phys.*, 1976, **65**, 438.
21 M. P. Fülscher, K. Andersson and B. O. Roos, *J. Chem. Phys.*, 1992, **96**, 9204.
22 M. P. Fülscher and B. O. Roos, *Theor. Chim. Acta*, 1994, **87**, 403.
23 J. E. Del Bene, J. D. Watts and R. J. Bartlett, *J. Chem. Phys.*, 1997, **106**, 6051.
24 P. Weber and J. R. Reimers, *J. Phys. Chem. A*, 1999, **103**, 9821.
25 P. Weber and J. R. Reimers, *J. Phys. Chem. A*, 1999, **103**, 9830.
26 Y. Li, J. Wan and X. Xu, *J. Comp. Chem.*, 2007, **28**, 1658.
27 C. Woywod, A. Papp, G. J. Halász and A. Vibók, *Theor. Chem. Acc.*, 2010, **125**, 521.
28 R. Schneider and W. Domcke, *Chem. Phys. Lett.*, 1988, **150**, 235.
29 R. Schneider and W. Domcke, *Chem. Phys. Lett.*, 1989, **159**, 61.
30 U. Manthe and H. Köppel, *J. Chem. Phys.*, 1990, **93**, 1658.
31 R. Seidner, G. Stock, A. L. Sobolewski and W. Domcke, *J. Chem. Phys.*, 1991, **96**, 5298.
32 C. Woywod, W. Domcke, A. L. Sobolewski and H.-J. Werner, *J. Chem. Phys.*, 1994, **100**, 1400.
33 G. Stock, C. Woywod, W. Domcke, T. Swinney and B. H. Hudson, *J. Chem. Phys.*, 1995, **103**, 6851.
34 T. Shiozaki, C. Woywod and H.-J. Werner, *Phys. Chem. Chem. Phys.*, 2013, **15**, 262.
35 M. Sala, B. Lasorne, F. Gatti and S. Guérin, *Phys. Chem. Chem. Phys.*, 2014, **16**, 15957.
36 M. Kanno, Y. Ito, N. Shimakura, S. Koseki, H. Kono and Y. Fujimura, *Phys. Chem. Chem. Phys.*, 2015, **17**, 2012.
37 G. A. Worth, H.-D. Meyer and L. S. Cederbaum, *J. Chem. Phys.*, 1996, **105**, 4412.
38 G. A. Worth, H.-D. Meyer and L. S. Cederbaum, *J. Chem. Phys.*, 1998, **109**, 3518.
39 G. A. Worth, H.-D. Meyer and L. S. Cederbaum, *Chem. Phys. Lett.*, 1999, **299**, 451.
40 A. Raab, G. A. Worth, H.-D. Meyer and L. S. Cederbaum, *J. Chem. Phys.*, 1999, **110**, 936.
41 O. Vendrell and H.-D. Meyer, *J. Chem. Phys.*, 2011, **134**, 044135.
42 T. Westermann and U. Manthe, *J. Chem. Phys.*, 2012, **137**, 22A509.
43 M. Thoss, W. H. Miller and G. Stock, *J. Chem. Phys.*, 2000, **112**, 10282.
44 M. Santer, U. Manthe and G. Stock, *J. Chem. Phys.*, 2001, **114**, 2001.
45 K. Ando and M. Santer, *J. Chem. Phys.*, 2003, **118**, 10399.
46 D. V. Shalashilin and M. S. Child, *J. Chem. Phys.*, 2004, **121**, 3563.
47 P. Puzari, R. S. Swathi, B. Sarkar and S. Adhikari, *J. Chem. Phys.*, 2005, **123**, 134317.
48 P. Puzari, B. Sarkar and S. Adhikari, *J. Chem. Phys.*, 2006, **125**, 194316.
49 X. Chen and V. S. Batista, *J. Chem. Phys.*, 2006, **125**, 124313.
50 I. Burghardt, K. Giri and G. A. Worth, *J. Chem. Phys.*, 2008, **129**, 174104.
51 C. Lasser and T. Swart, *J. Chem. Phys.*, 2008, **129**, 034302.
52 U. Werner, R. Mitrić, T. Suzuki and V. Bonačić-Koutecký, *Chem. Phys.*, 2008, **349**, 319.
53 D. V. Shalashilin, *J. Chem. Phys.*, 2010, **132**, 244111.
54 G. Tomasello, A. Humeniuk and R. Mitrić, *J. Phys. Chem. A*, 2014, **118**, 8437.
55 L. Wang, H.-D. Meyer and V. May, *J. Chem. Phys.*, 2006, **125**, 014102.

56 M. Sukharev and T. Seideman, *Phys. Rev. Lett.*, 2004, **93**, 093004.
57 M. Sukharev and T. Seideman, *Phys. Rev. A*, 2005, **71**, 012509.
58 T. J. Penfold, G. A. Worth and C. Meier, *Phys. Chem. Chem. Phys.*, 2010, **12**, 15616.
59 P. S. Christopher, M. Shapiro and P. Brumer, *J. Chem. Phys.*, 2005, **123**, 064313.
60 P. S. Christopher, M. Shapiro and P. Brumer, *J. Chem. Phys.*, 2006, **125**, 124310.
61 I. Thanopulos, X. Li, P. Brumer and M. Shapiro, *J. Chem. Phys.*, 2012, **137**, 064111.
62 M. Sala, M. Saab, B. Lasorne, F. Gatti and S. Guérin, *J. Chem. Phys.*, 2014, **140**, 194309.
63 M. Saab, M. Sala, B. Lasorne, F. Gatti and S. Guérin, *J. Chem. Phys.*, 2014, **141**, 134114.
64 A. L. Sobolewski, C. Woywod and W. Domcke, *J. Chem. Phys.*, 1993, **98**, 5627.
65 I. J. Palmer, I. N. Ragazos, F. Bernardi, M. Olivucci and M. A. Robb, *J. Am. Chem. Soc.*, 1993, **115**, 673.
66 G. A. Worth, *J. Photochem. Photobiol. A*, 2007, **190**, 190.
67 G. A. Worth, R. E. Carley and H. H. Fielding, *Chem. Phys.*, 2007, **338**, 220.
68 B. Lasorne, F. Silicia, M. J. Bearpark, M. A. Robb, G. A. Worth and L. Blancafort, *J. Chem. Phys.*, 2008, **128**, 124307.
69 B. Lasorne, M. J. Bearpark, M. A. Robb and G. A. Worth, *J. Phys. Chem. A*, 2008, **112**, 13017.
70 D. S. N. Parker, R. S. Minns, T. J. Penfold, G. A. Worth and H. H. Fielding, *Chem. Phys. Lett.*, 2009, **469**, 43.
71 T. J. Penfold and G. A. Worth, *J. Chem. Phys.*, 2009, **131**, 064303.
72 R. S. Minns, D. S. N. Parker, T. J. Penfold, G. A. Worth and H. H. Fielding, *Phys. Chem. Chem. Phys.*, 2010, **12**, 15607.
73 T. J. Penfold, R. Spesyvtsev, O. M. Kirkby, R. S. Minns, D. S. N. Parker, H. H. Fielding and G. A. Worth, *J. Chem. Phys.*, 2012, **137**, 204310.
74 H.-D. Meyer, U. Manthe and L. S. Cederbaum, *Chem. Phys. lett.*, 1990, **165**, 73.
75 U. Manthe, H.-D. Meyer and L. S. Cederbaum, *J. Chem. Phys.*, 1992, **97**, 3199.
76 H.-D. Meyer and G. A. Worth, *Theor. Chem. Acc.*, 2003, **109**, 251.
77 H.-D. Meyer, F. Gatti and G. A. Worth, *Multidimensional Quantum Dynamics: MCTDH Theory and Applications*, Wiley-VCH, Weinheim, 2009.
78 H. Köppel, W. Domcke and L. S. Cederbaum, *Adv. Chem. Phys.*, 1984, **54**, 59.
79 A. A. Granovsky, *J. Chem. Phys.*, 2011, **134**, 214113.
80 G. A. Worth and L. S. Cederbaum, *Annu. Rev. Phys. Chem.*, 2004, **55**, 127.
81 D. R. Yarkony, *Chem. Rev.*, 2012, **112**, 481.
82 R. A. Kendall, T. H. Dunning Jr. and R. J. Harrison, *J. Chem. Phys.*, 1992, **96**, 6796.
83 M. J. Frisch, G. W. Trucks, H. B. Schlegel, G. E. Scuseria, M. A. Robb, J. R. Cheeseman, J. A. Montgomery, Jr., T. Vreven, K. N. Kudin, J. C. Burant, J. M. Millam, S. S. Iyengar, J. Tomasi, V. Barone, B. Mennucci, M. Cossi, G. Scalmani, N. Rega, G. A. Petersson, H. Nakatsuji, M. Hada, M. Ehara, K. Toyota, R. Fukuda, J. Hasegawa, M. Ishida, T. Nakajima, Y. Honda, O. Kitao, H. Nakai, M. Klene, X. Li, J. E. Knox, H. P. Hratchian, J. B. Cross, V. Bakken, C. Adamo, J. Jaramillo, R. Gomperts, R. E. Stratmann, O. Yazyev, A. J. Austin, R. Cammi, C. Pomelli, J. W. Ochterski, P. Y. Ayala, K. Morokuma, G. A. Voth, P. Salvador, J. J. Dannenberg, V. G. Zakrzewski, S. Dapprich, A. D. Daniels, M. C. Strain, O. Farkas, D. K. Malick, A. D. Rabuck, K. Raghavachari, J. B. Foresman, J. V. Ortiz, Q. Cui, A. G. Baboul, S. Clifford, J. Cioslowski, B. B. Stefanov, G. Liu, A. Liashenko, P. Piskorz, I. Komaromi, R. L. Martin, D. J. Fox, T. Keith, M. A. Al-Laham, C. Y. Peng, A. Nanayakkara, M. Challacombe, P. M. W. Gill, B. Johnson, W. Chen, M. W. Wong, C. Gonzalez and J. A. Pople, Gaussian, Inc., Wallingford, CT, 2004.
84 A. A. Granovsky, *Firefly version 7.1.G*, `http://classic.chem.msu.su/gran/firefly/index.html`.
85 M. W. Schmidt, K. K. Baldridge, J. A. Boatz, S. T. Elbert, M. S. Gordon, J. H. Jensen, S. Koseki, N. Matsunaga, K. A. Nguyen, S. Su, T. L. Windus, M. Dupuis and J. A. Montgomery, *J. Comput. Chem.*, 1993, **14**, 1347.
86 E. Epifanovsky, I. Polyakov, B. Grigorenko, A. Nemukhin and A. I. Krylov, *J. Chem. Phys.*, 2010, **132**, 115104.
87 I. V. Polyakov, B. L. Grigorenko, E. M. Epifanovsky, A. I. Krylov and A. V. Nemukhin, *J. Chem. Theo. Comput.*, 2010, **6**, 2377.
88 B. L. Grigorenko, A. V. Nemukhin, D. I. Morozov, I. V. Polyakov, K. B. Bravaya and A. I. Krylov, *J. Chem. Theo. Comput.*, 2011, **8**, 1912.
89 B. L. Grigorenko, A. V. Nemukhin, I. V. Polyakov and A. I. Krylov, *J. Phys. Chem. Lett.*, 2013, **4**, 1743.
90 P. M. Kozlowski, T. Kamachi, M. Kumar, T. Nakayama and K. Yoshizawa, *J. Phys. Chem. B*, 2010, **114**, 5928.
91 A. Udvarhelyi and T. Domratcheva, *J. Photochem. Photobiol. A*, 2011, **87**, 554.
92 I. Ioffe, A. L. Dobryakov, A. A. Granovsky, N. P. Ernsting and J. L. Pérez Lustres, *ChemPhysChem*, 2011, **12**, 1860.
93 A. V. Bochenkova and L. H. Andersen, *Faraday Discuss.*, 2013, **163**, 297.
94 K. Kornobis, N. Kumar, B. M. Wong, P. Lodowski, M. Jaworska, T. Andruni, K. Ruud and P. M. Kozlowski, *J. Phys. Chem. A*, 2011, **115**, 1280.
95 S. Gozem, M. Huntress, I. Schapiro, R. Lindh, A. A. Granovsky, C. Angeli and M. Olivucci, *J. Chem. Theo. Comput.*, 2012, **8**, 4069.
96 S. Gozem, F. Melaccio, R. Lindh, A. I. Krylov, A. A. Granovsky, C. Angeli and M. Olivucci, *J. Chem. Theo. Comput.*, 2013, **9**, 4495.
97 S. Gozem, F. Melaccio, A. Valentini, M. Filatov, M. Huix-Rotllant, N. Ferré, L. M. Frutos, C. Angeli, A. I. Krylov, A. A. Granovsky, R. Lindh and M. Olivucci, *J. Chem. Theo. Comput.*, 2014, **10**, 3074.
98 S. P. Neville and G. A. Worth, *J. Chem. Phys.*, 2014, **140**, 034317.
99 B. Lasorne, J. Jornet-Somoza, H.-D. Meyer, D. Lauvergnat, M. A. Robb and F. Gatti, *Spectrochim. Acta, Part A*, 2014, **119**, 52.
100 M. R. Silva-Junior, M. Schreiber, S. P. A. Sauer and W. Thiel, *J. Chem. Phys.*, 2010, **133**, 174318.
101 M. Schreiber, M. R. Silva-Junior, S. P. A. Sauer and W. Thiel, *J. Chem. Phys.*, 2008, **128**, 134110.
102 C. Cattarius, G. A. Worth, H.-D. Meyer and L. S. Cederbaum, *J. Chem. Phys.*, 2001, **115**, 2088.
103 F. Wang, S. P. Neville, R. Wang and G. A. Worth, *J. Phys. Chem. A*, 2013, **117**, 7298.
104 O. P. J. Vieuxmaire, Z. Lan, A. L. Sobolewski and W. Domcke, *J. Chem. Phys.*, 2008, **129**, 224307.
105 M. Sala, O. M. kyrkby, S. Guérin and H. H. Fielding, *Phys. Chem. Chem. Phys.*, 2014, **16**, 3122.
106 G. A. Worth, M. H. Beck, A. Jäckle and H.-D. Meyer, The MCTDH Package, Version 8.2, (2000). H.-D. Meyer, Version 8.3 (2002), Version 8.4 (2007). See http://mctdh.uni-hd.de.
107 E. V. Gromov, V. Sivaranjana Reddy, F. Gatti and H. Köppel, *J. Chem. Phys.*, 2013, **139**, 234306.
108 L. Joubert-Doriol, B. Lasorne, D. Lauvergnat, H.-D. Meyer and F. Gatti, *J. Chem. Phys.*, 2014, **140**, 044301.
109 M. Saab, L. Joubert-Doriol, B. Lasorne, S. Guérin and F. Gatti, *Chem. Phys.*, 2014, **442**, 93.
110 F. Richter, F. Gatti, C. Léonard, F. Le Quéré and H.-D. Meyer, *J. Chem. Phys.*, 2007, **127**, 164315.
111 G. Pasin, C. Iung, F. Gatti, F. Richter, C. Léonard and H.-D. Meyer, *J. Chem. Phys.*, 2008, **129**, 144304.
112 M. Sala, F. Gatti, D. Lauvergnat and H.-D. Meyer, *Phys. Chem. Chem.*

Phys., 2012, **14**, 3791.
113 O. Vendrell, F. Gatti and H.-D. Meyer, *Angew. Chem. Int. Ed.*, 2007, **46**, 6918.
114 M. Schröder and H.-D. Meyer, *J. Chem. Phys.*, 2014, **141**, 034116.
115 T. Westermann, J. B. Kim, M. L. Weichman, C. Hock, T. I. Yacovitch, J. Palma, D. M. Neumark and U. Manthe, *Angew. Chem. Int. Ed.*, 2014, **53**, 1122.
116 M. Sala, S. Guérin, F. Gatti, R. Marquardt and H.-D. Meyer, *J. Chem. Phys.*, 2012, **136**, 194308.
117 M. Sala, F. Gatti and S. Guérin, *J. Chem. Phys.*, 2014, **141**, 164326.
118 A. Perveaux, D. Lauvergnat, F. Gatti, M. A. Robb, G. J. Halász, A. Vibók and B. Lasorne, *J. Phys. Chem. A*, 2014, **118**, 8773.
119 J. C. Light, I. P. Hamilton and J. V. Lill, *J. Chem. Phys.*, 1985, **82**, 1400.